JOURNAL OF THEORETICAL
AND APPLIED MECHANICS
https://doi.org/10.15632/jtam-pl/225472
ONLINE FIRST

ANALYTICAL FORMULAE FOR 2D BALLISTIC LIMIT CURVES OVER A RANGE OF MATERIAL THICKNESSES BASED ON THE RECHT–IPSON MODEL AND SYMBOLIC REGRESSION

Tomasz HACHAJ[1], Teresa FRAS[2*]

[1] *Faculty of Electrical Engineering, Automatics, Computer Science and Biomedical Engineering, AGH University, Krakow, Poland*
[2] *French-German Research Institute of Saint-Louis (ISL), Saint-Louis, France*
[*]corresponding author, *teresa.fras@isl.eu*

The study discusses an application of the physics-aware symbolic regression (PASR) paradigm, with the embedded Recht–Ipson (R-I) model, to describe the relationship between the 7.62 mm AP P80 projectile's initial impact and the residual velocities of the S355 steel plates of varying thicknesses. The present approach results in a straightforward analytical "SR R-I" formula, which can be easily applied in engineering practice to determine ballistic limit curves and velocities (BLCs and BLVs). The proposed approach has demonstrated statistical effectiveness that outperforms other machine learning (ML) algorithms in both fitting accuracy and the predictive capability of these terminal ballistic features.

Keywords: terminal ballistics; machine learning; symbolic regression; Recht–Ipson; ballistic limit curves.

1. Introduction

Numerical modelling in terminal ballistics is a well-established approach that has been covered extensively over many decades in numerous papers, books, and surveys (Anderson Jr. & Bodner, 1988; Rosenberg & Dekel, 2012). More recently, machine learning (ML) methods, alongside traditional mathematical modelling using numerical methods – including the finite element method (FEM) – have become an integral part of the researcher's toolkit and engineering practice in materials sciences, particularly in terminal ballistics. ML modelling, especially physics-informed models, (Karniadakis *et al.*, 2021), has been proven successful for predicting high-complexity, high-dimensional problems such as the V50 ballistic limit and the depth of projectile penetration (Rietkerk *et al.*, 2023; Ryan *et al.*, 2024). In (Hachaj & Frąś, 2026), the stochastic physics-based oversampling methods are investigated in order to improve ML-based approximation of 2D ballistic limit curves (BLCs). In that work, we proposed a data-driven ML method to approximate BLCs as functions of material thickness and impact velocity, combining experimental data, finite element simulations, and stochastic physics-based oversampling. A novel oversampling approach is introduced that leverages physical knowledge (via derivatives of fitted ballistic models) to generate more informative training data, thereby improving pre-

Ministry of Science and Higher Education Republic of Poland
WEKTORY NAUKI

This publication has been funded by the Polish Ministry of Science and Higher Education under the "Vectors of Science" programme, project number WNK/SN/0508/2025/01, with project funding of PLN 134,200.00 and total project value of PLN 174,200.00.
The content of this article was presented during the 62nd Symposium "Modelowanie w mechanice" (Modelling in Mechanics), Szczyrk, Poland, March 1–4, 2026.

diction accuracy compared to uniform sampling. The results show that deep neural networks trained with this approach can accurately predict both curve shapes and ballistic limit velocities (BLVs) for unseen material thicknesses, reducing the need for costly experiments. ML ballistic modelling for various materials is a relatively new subject of research. It has already been applied to aluminium, titanium, and steel targets (Ryan *et al.*, 2024); initial studies also examine the reverse prediction of impact parameters for 3D woven fabrics subjected to ballistic impact using deep learning methods (Li *et al.*, 2026).

Several studies have applied artificial neural networks (ANNs) to predict residual velocity. Husain *et al.* (2024) used input velocity, shape factor, and target thickness, whereas Deng *et al.* (2025) employed angle, target thickness, and initial velocity. However, neither study evaluated the ability of their models to predict BLV for unknown material thickness, which is among the most important tasks of terminal ballistics.

A major limitation of popular ML approaches, such as neural networks, support vector machines, and classifier and regressor ensembles, is their limited interpretability. In particular, it is often difficult to understand why these models produce specific outputs, how sensitive their predictions are to variations in the training data, and whether their behavior remains stable and consistent across different input conditions. Moreover, these models do not inherently guarantee compliance with known physical laws, which can be critical in scientific and engineering applications. These limitations have driven the rapid development of Explainable Artificial Intelligence (XAI), an important branch of modern machine learning (Dwivedi *et al.*, 2023; Hachaj & Piekarczyk, 2025). The primary objective of XAI is to design models and methodologies whose decision-making processes can be understood, analysed, and trusted by users. This includes providing insights into feature importance, model sensitivity, and the reasoning behind predictions, thereby improving transparency, reliability, and the integration of domain knowledge into data-driven approaches.

Symbolic regression (SR) is a regression algorithm that offers easy-to-interpret results. This technique involves explicit mathematical expressions that best fit a dataset without assuming a predefined model structure. It is often implemented with methods such as genetic programming, which evolve formulas that balance accuracy and simplicity, leading to more intuitive interpretations of the results. SR can also be used to address and interpret terminal ballistic experiments. Levadnyi *et al.* (2024) investigated numerically and experimentally the ballistic performance of thermoplastic polyurethane (TPU)/steel configurations against spherical projectiles and used SR to derive the final equation. Abid *et al.* (2025) and Zou *et al.* (2025) developed an SR-based equation for predicting the depth of penetration for targets under high-velocity projectile impact. Zhang *et al.* (2026) discussed the SR-based impact fracture model. Saifoori *et al.* (2025) linked the impact deformation of elastic-perfectly plastic particles to their material properties and impact velocity using SR.

In this paper, building on our previous work, we propose a method for deriving analytical formulae for 2D BLCs over a range of material thicknesses using SR, enabling the resulting model to be directly interpreted and applied by users. To the best of our knowledge, the application of SR to the problem of 2D limit curves estimation has not yet been published in the literature, and the results we have obtained are pioneering in this field.

2. Problem formulation

The BLC describes the relationship between a projectile's initial velocity and its residual velocity after perforating the target. It is a simplified characterization of both the projectile's penetration capability and the tested material's resistance to ballistic impacts. To approximate the relation between the projectile's velocities and, therefore, to determine the BLC of the impact configuration, the Recht–Ipson (R-I) model is often used (Frąś *et al.*, 2011; Karl *et al.*, 2020; Recht & Ipson, 1963).

$$v_r \approx \text{R-I}(v_i, a, p) = \begin{cases} a \cdot (v_i^p - {v_{bl}}^p)^{1/p} & \text{if} \quad v_i \geq v_{bl}, \\ 0 & \text{if} \quad v_i < v_{bl}, \end{cases} \tag{2.1}$$

where v_i is the initial velocity, v_r is the residual velocity, v_{bl} is the BLV, i.e., the minimum impact velocity required for a projectile to perforate a target (typically determined through impact experiments), parameters a, p are fitted from experimental data by a numeric solver (Deng *et al.*, 2025), for example, non-linear least squares with bounds or the generalized reduced gradient method (Lasdon *et al.*, 1974).

Figure 1a shows the set of BLCs and BLVs obtained experimentally for S355 steel plates with thicknesses of 8 mm and 16 mm. The S355 structural steel is a low-alloy carbon-manganese steel with guaranteed minimum mechanical properties and satisfactory ductility, as shown in Table 1. This steel grade is used in a wide range of construction and structural applications, thanks to its good welding properties and guaranteed strength.

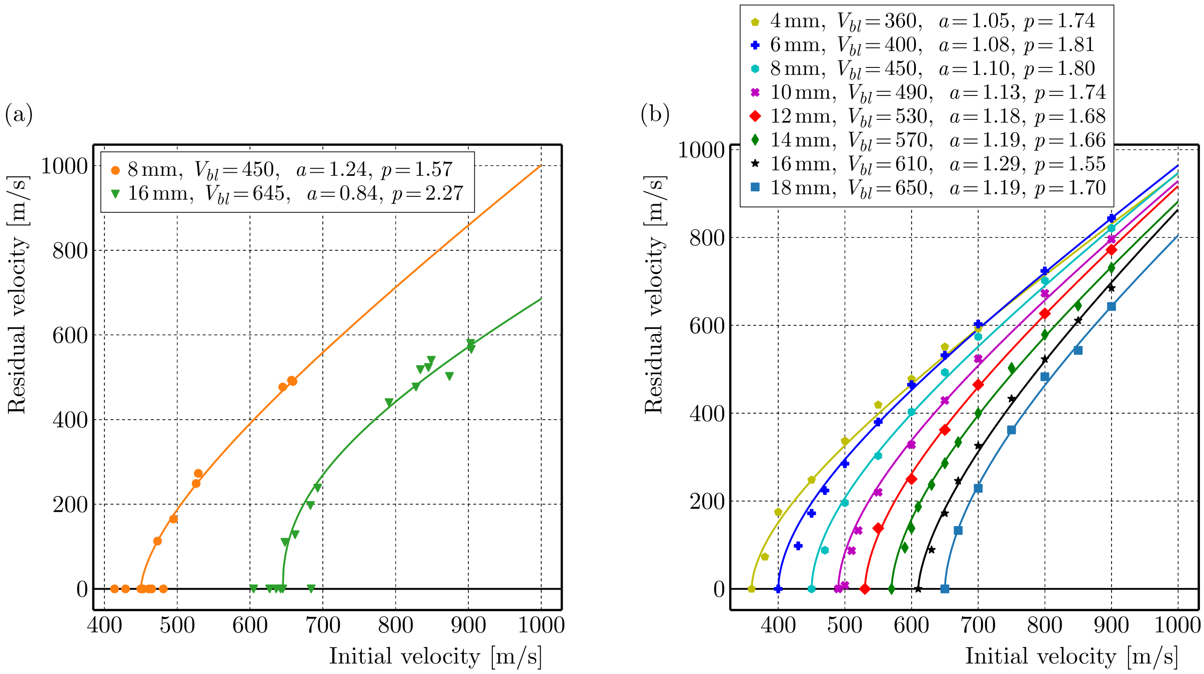

Fig. 1. Our dataset S355 vs. 7.62 mm × 51 mm AP P80 impacts at 0° NATO with BLC fitted to the data: (a) a plot of experimental data; (b) a numeric simulation result. The legends in both plots include parameters of Eq. (2.1).

Table 1. Properties of the S355 structural steel with nominal thickness $t \leq 40$ mm (European Committee for Standardization, 2019).

Property	Value
Density	7850 kg/m^3
Young's modulus	210 GPa
Shear modulus	81 GPa
Poisson's ratio	0.3
Coefficient of linear thermal expansion	12×10^{-6} K^{-1}
Yield strength	355 MPa
Ultimate strength	490 MPa

The S355 steel plates were impacted by 7.62 mm × 51 mm P80 (0.308 Win) armour-piercing rounds. In the cases where the plates were perforated, the projectile cores were not fragmented. The craters left after projectile passage have diameters that closely match the core diameter, i.e., about 5.2 mm to 5.5 mm. Figure 1b presents the numerical approximations of these curves, along with the curves determined numerically for other steel plate thicknesses. The R-I model parameters are shown in the figures. The methodology for establishing the BLCs is detailed in (Hachaj & Frąś, 2026). In the current study, the BLCs' origins and the manner of their numerical representation are not of primary importance. The experimental data were used to fit the numerical experiments, ensuring they reflected the material's actual behaviour. In the legends in both plots, we also list parameters of Eq. (2.1). We have used the standard pyplot library to plot residual velocity against projectile impact velocity, a commonly used approach among researchers (Wei *et al.*, 2024). As a result, many of those plots are very similar in appearance. The parameter-fitting problem was solved using a numerical solver that minimizes the mean-squared error of the residuals from a nonlinear model. When fitting multiple parameters, as in the R-I equation, it is common to obtain solutions with similar errors for different values of the selected parameters. This occurs because the optimization procedure seeks to minimize the error between the observed and predicted values, subject to constraints on the parameter ranges, rather than to ensure the repeatability of the curve parameters, where some of them do not have an individual physical interpretation. In our case, the parameters a and p obtained for the experimental and numerical results have different values, but we did not directly refer to them in the further analysis, taking the R-I equations as the reference, not their individual parameters.

As can be concluded from Fig. 1, the R-I model can be applied only to a single material thickness. Therefore, to obtain BLCs and BLVs over a wider range of target thicknesses, multiple impact experiments must be conducted. As discussed earlier, some studies demonstrate the successful application of ML algorithms to generalize the R-I approximation and to predict data not included in the training dataset. However, there remains a lack of easily interpretable analytical solutions that can be applied directly, without the need for complex software packages that produce results in a black-box manner. In this study, we propose a method for deriving an analytical formula based on the R-I model to describe the performance of S355 steel plates over a wider thickness range under the impact of 7.62 mm AP P80 projectiles.

2.1. Designing optimized formula for SR

Our goal is to obtain an analytic formula for 2D BLCs over a range of material thicknesses, in which residual velocity v_r is a function of input velocity of projectile v_i and material thickness t for a given material. The straightforward approach is to apply SR directly to the dataset and let it fit the training data, imposing constraints on the solution's complexity to prevent overfitting. A major limitation of this approach is that the final solution is likely to be physically inconsistent and very difficult (or even impossible) to interpret using materials science. We will call this unconstrained approach an SR model.

The other approach is to use a physics-aware symbolic regression (PASR) algorithm (El Hasadi & Elghannay, 2026) in which known physics, expressed as symbolic relations, is embedded into the search space. In our case, we want the symbolic solution to have the following form, derived from (2.1):

$$\widehat{v_r}(v_i,t) = \mathcal{a}(t)\cdot\left(v_i^{\mathcal{p}(t)} - \mathcal{v}_{\mathcal{bl}}(t)^{\mathcal{p}(t)}\right)^{1/(p(t))}, \qquad v_i \geq \mathcal{v}_{\mathcal{bl}}(t), \tag{2.2}$$

where $\mathcal{a}(t)$, $\mathcal{p}(t)$, and $\mathcal{v}_{\mathcal{bl}}(t)$ are terms a, b, v_{bl} from the original R-I formula, extended to be functions of material thickness t. By making this assumption, the SR solution will have an intuitive, easy-to-explain form, more closely aligned with known physical models. We will call this algorithm setting an SR R-I model.

In order to find an analytic formula with symbolic regression for both SR and SR R-I in the optimization process, we used a set of binary operators $\circ$ for addition, subtraction, multiplication, division, and exponentiation:

$$x \circ y \in \left\{ x + y,\ x \cdot y,\ x^y,\ \frac{x}{y} \right\}. \tag{2.3}$$

We used unary operators u square, cube, natural logarithm, base-2 logarithm, base-10 logarithm, square root, inverse, and natural logarithm of argument plus one:

$$u(x) = \left\{ x^2, x^3, \ln(x), \log_2(x), \log_{10}(x), \sqrt{x}, \frac{1}{x}, \ln(x+1) \right\}. \tag{2.4}$$

We chose these because they are commonly used operators that allow us to model linear, polynomial, exponential, and logarithmic relationships. Some unary operators can be expressed using binary operators, and some unary operators can be derived from other unary operators; however, to simplify the genetic algorithm's search of the space of potential solutions, we used them directly. We have also added constraints on power values to limit the complexity to 3 (the base of power has no constraint), to avoid overly complex exponential functions. We use the square error loss function. We limited the complexity of the SR solution to 30 terms and the SR R-I to 20 terms. In the SR R-I approach, we provide the genetic algorithm with a significant hint regarding the general form of the final solution. To avoid generating overly complex solutions, we arbitrarily limited the search to 20 terms. In contrast, an SR algorithm without such a preliminary hint would be highly unlikely to find a solution as well-suited to the data as SR R-I when restricted to just 20 terms. Therefore, for this comparison, we set the maximum allowed solution length to 30 terms. Both the base-2 logarithm and the base-10 logarithm can be replaced by the quotient of the corresponding natural logarithms; however, we have deliberately defined these two additional logarithms as base functions in Eq. (2.4). This is due to the fact that the genetic algorithm, which is the main mechanism on which SR is based, "does not know" these formulas for conversion, and changing the logarithm base always requires the use of three operations in the final formula in the solution: division and the addition of the appropriate logarithmic operation in both the numerator and the denominator. This increases the solution's complexity, and since we use the Pareto front, we want the solutions to be as accurate as possible while remaining as simple as possible (with a small number of components). It is also very unlikely that a formula for converting logarithm bases would be found precisely by a genetic algorithm. For this reason, we decided to explicitly define logarithms with three commonly used bases.

We generated a training dataset using stochastic physics-based oversampling with cumulative distribution function (CDF), which is defined with equations (Hachaj & Frąś, 2026):

$$F_{v_i}(y) = P(v_i \leq y) = \frac{\int_{b_1}^{y} g(v_i)_{[b_1,b_2]} dv_i}{\int_{b_1}^{b_2} g(v_i)_{[b_1,b_2]} dv_i}, \tag{2.5}$$

$$g(v_i)_{[b_1,b_2]} = c_1 + c_2 \cdot \left| \frac{\partial v_r(v_i)}{\partial v_i} \right| + c_3 \cdot \left| \frac{\partial^2 v_r(v_i)}{\partial v_i^2} \right|, \tag{2.6}$$

where $v_i \in [b_1, b_2] \wedge\ c_1 + c_2 + c_3 = 1 \wedge\ c_1, c_2, c_3 \in [0, 1]$, and $||$ is the absolute value.

In our case $[b_1, b_2] = [v_{bl}(t), 1000]$, which is a relevant range of speeds [m/s] for our dataset. $v_{bl}(t)$ is the BLV for a given material thickness. In both the experiments and the FEM simulations, these values correspond to the minimum impact velocity at which a 7.62 mm P80 projectile perforated the tested targets. Moreover, 100 data points were generated for each thickness to produce a uniquely defined ballistic-limit curve. $[c_1, c_2, c_3] = [0, 0.25, 0.75]$. v_r were previously fitted to experimental and numerical data as explained in Section 2. In Fig. 2, we present four

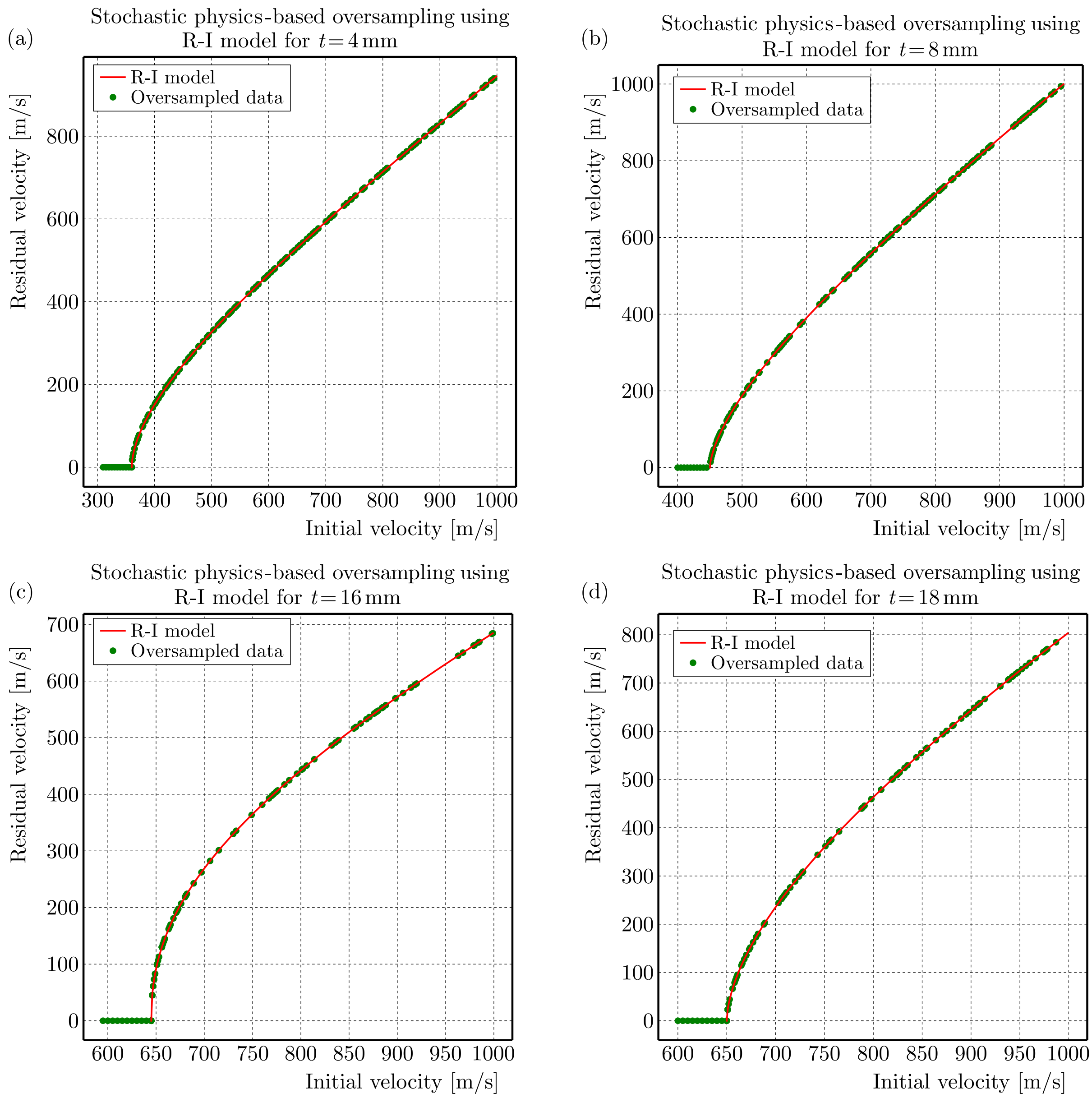

Fig. 2. Four example data series generated according to Eq. (2.5) on our dataset with the setup described in Subsection 2.1. Red line represents the reference R-I model; green points are random samples used during the training of all ML models.

example data series generated according to Eq. (2.5) from our dataset. The validation (test) dataset consists of original data points from experiments and numerical simulations (see Fig. 1). The exact validation procedure will be discussed in Section 3.

2.2. Comparison with other machine learning models

Several other ML models have been successfully used in materials science tasks, particularly for solving ballistic problems. Among them are extreme gradient boosting (XGBoost) and random forest (RF), which were used for predicting the outcome of terminal ballistics events, namely ballistic limit and penetration depth, as mentioned in (Abid *et al.*, 2025; Ryan *et al.*, 2024). Those two models are robust ensemble methods that incorporate many "weak" decision tree regressors. However, they apply different training strategies: XGBoost uses boosting, while RF applies bagging. The main issue with these two methods is the low level of explainability of the resulting models (XAI) due to the large number of decision trees in each model. Since these are state-of-the-art, "out of the box" methods that do not require a complicated setup for tasks of this type, we also trained these models on an oversampled dataset (the same as in the case of SR and SR R-I). We compared the results with those obtained from SRs.

3. Results

To validate our approach, we have implemented the methodology described in Section 2 and executed it on the dataset described in the same section. Implementation was done in Python 3.12. Among the most important packages we used were PySR 1.5.9 (Cranmer, 2023) for SR, scikit-learn 1.8.0 for RF regression, XGBoost 3.2.0 for XGBoost regression, SciPy 1.17.1 for statistical evaluation, and NumPy 2.4.2 for general-purpose algebra. Hyperparameters for all ML methods were determined experimentally, and we will not discuss them here due to paper space limitations. The source code was executed on a PC with an Intel i7-9700 3.00 GHz CPU, 64 GB RAM, an NVIDIA GeForce RTX 2060 6 GB, and Windows OS[1]. The hyperparameters of all the ML methods used are available (see the footnote). The SR training for each leave-one-out case lasts about 10 minutes on our hardware, while RF and XGBoost take about several seconds. We have evaluated SR ("basic" algorithm without assuming constraints on final solution besides those mentioned in Subsection 2.1), SR R-I with constraints on solution represented by Eq. (2.2) (see Subsection 2.1), XGBoost, and RF (see Subsection 2.2).

To evaluate the obtained results, we used the following error functions:

- absolute error:
$$\mathrm{AE}(y_i, \widehat{y}_i) = |y_i - \widehat{y}_i|\,, \tag{3.1}$$
- relative error:
$$\mathrm{RE}(y_i, \widehat{y}_i) = \left|\frac{y_i - \widehat{y}_i}{y_i + \epsilon}\right|, \tag{3.2}$$
where ϵ is the small value that prevents division by zero (in our case, condition $y_i \geq 0$ is always true),
- root mean square error:
$$\mathrm{RMSE}(Y, \widehat{Y}) = \sqrt{\frac{1}{n}\sum_{i=1}^{n}(y_i - \widehat{y}_i)^2}, \tag{3.3}$$
- mean absolute error:
$$\mathrm{MAE}(Y, \widehat{Y}) = \frac{1}{n}\sum_{i=1}^{n}|y_i - \widehat{y}_i|\,, \tag{3.4}$$
- the R^2 score (coefficient of determination):
$$R^2(Y, \widehat{Y}) = 1 - \frac{\sum_{i=1}^{n}(y_i - \widehat{y}_i)^2}{\sum_{i=1}^{n}(y_i - \overline{y})^2}, \tag{3.5}$$
- mean relative error:
$$\mathrm{MRE}(Y, \widehat{Y}) = \frac{1}{n}\sum_{i=1}^{n}\left|\frac{y_i - \widehat{y}_i}{y_i + \epsilon}\right|. \tag{3.6}$$

[1] Source codes for our research can be downloaded from https://github.com/browarsoftware/symbolic_ballistic_recht_ipson (accessed March 4, 2026).

We used leave-one-out cross-validation, in which each thickness was used as the training dataset and the remaining thickness as the validation dataset. Due to this, there were 8 folds, for $t \in \{4, 6, 8, 10, 12, 14, 16, 18\}$ mm. For each of these solutions, we have evaluated how well the obtained curves approximate unknown data (generalization ability). The averaged results plus-minus standard deviations are presented in Table 2. For curves, we did not evaluate MRE because the experimental data near BLV had a near-stochastic character, and the relative error results there might be misleading. We have also checked how well the model approximates BLV for unknown data, which is also a generalization ability test. The results are presented in Table 3. Because we only have a single data series (a single BLV estimate for each thickness), the standard deviation is calculated only for MRE.

Table 2. Evaluation results of the models – how well curves approximate unknown data (generalization ability).

Metric	Model			
	SR	SR R-I	RF	XGBoost
RMSE	51.656 ±38.218	52.504 ±47.586	93.856 ±41.229	94.952 ±40.59
MAE	47.071 ±37.509	46.248 ±44.058	82.269 ±43.867	83.264 ±42.965
R^2	0.908 ±0.116	0.894 ±0.176	0.770 ±0.216	0.768 ±0.212

Table 3. Evaluation results of the models – how well the models approximate BLV for unknown data (generalization ability).

Metric	Model			
	SR	SR R-I	RF	XGBoost
MRE	0.043 ±0.055	0.028 ±0.029	0.094 ±0.020	0.08 ±0.034
RMSE	32.697	25.678	50.061	42.702
MAE	20.375	16.641	47.875	39.000
R^2	0.894	0.934	0.751	0.819

To check whether the approximated results differ statistically, we have used a non-parametric Wilcoxon test, which does not assume that the results follow a normal distribution. We have tested whether the distribution of errors for one examined ML method is stochastically less than that of a second ML method. If $p < 0.05$, we have concluded that the error groups differ significantly. Because there is a high variance in the error groups visible in Table 2 and Table 3 that are mainly present in extrapolated curves, to ensure the reliability of the test, we have removed the single largest error value (possible outlier) and the corresponding error value from the other data series used for comparison. For this reason, the set of errors being compared was reduced by one value if the maximum error occurred at the same positions in both series, or by two values if it occurred at different positions. In Table 4, Table 5, Table 6, and Table 7, we present the p-values of the Wilcoxon test for RMSE and MAE (see Table 2) and for RE and AE (see Table 3).

In Fig. 3, we present an approximation of BLCs of all four ML methods trained on all but one thickness from our dataset that predict the shape BLC for the thickness that was not present in the dataset. We chose thicknesses of 8 mm and 16 mm because they predict the experimental data, and 4 mm and 18 mm because, in this setting, they visualize the extrapolation ability of algorithms. Red lines correspond to the reference R-I model curve fitted to data marked as red stars, and green lines are the ML model approximation.

In Fig. 4, we present visualizations of $\widehat{v_r}(v_i, t)$ from Eq. (2.2) as a surface plot. As mentioned, ML methods were trained on all but one thickness in our dataset to predict the shape BLC for

Table 4. p-values of the Wilcoxon test for RMSE (see Table 2). Boldface indicates $p < 0.05$, corresponding to statistically significant differences between the error distributions.

Model 1	Model 2			
	SR	SR R-I	RF	XGBoost
SR	1.000	0.578	**0.039**	**0.039**
SR R-I	0.500	1.000	**0.016**	**0.016**
RF	0.977	1.00	1.000	0.469
XGBoost	0.977	1.000	0.594	1.000

Table 5. p-values of the Wilcoxon test for MAE (see Table 2). Boldface indicates $p < 0.05$, corresponding to statistically significant differences between the error distributions.

Model 1	Model 2			
	SR	SR R-I	RF	XGBoost
SR	1.000	0.578	0.148	0.148
SR R-I	0.500	1.000	**0.016**	**0.016**
RF	0.891	1.000	1.000	0.406
XGBoost	0.891	1.000	0.656	1.000

Table 6. p-values of the Wilcoxon test for RE (see Table 3). Boldface indicates $p < 0.05$, corresponding to statistically significant differences between the error distributions.

Model 1	Model 2			
	SR	SR R-I	RF	XGBoost
SR	1.000	0.781	**0.008**	**0.008**
SR R-I	0.281	1.000	**0.016**	**0.016**
RF	1.000	1.000	1.000	1.000
XGBoost	1.000	1.000	1.000	1.000

Table 7. p-values of the Wilcoxon test for AE (see Table 3). Boldface indicates $p < 0.05$, corresponding to statistically significant differences between the error distributions.

Model 1	Model 2			
	SR	SR R-I	RF	XGBoost
SR	1.000	0.719	**0.031**	**0.031**
SR R-I	0.344	1.000	**0.016**	**0.016**
RF	0.984	1.000	1.000	1.000
XGBoost	0.984	1.000	1.000	1.000

the missing thickness. We have chosen to show the training results for the unknown $t = 8$ mm (experimental data).

SR algorithms return a set of potential solutions rather than a single one. Among them, we have selected the simplest (lowest-complexity) solutions, which, in the case of SR, incorporate both t and v_i with a loss value at most $2 \cdot 10^3$. This loss value was selected empirically. In the case of SR R-I, we have selected the simplest solutions (with lowest complexity), which incorporated t in either $\mathscr{a}(t)$ or $\mathscr{p}(t)$ and obligatorily in $v_{\mathscr{bl}}(t)$ with loss value at most $2 \cdot 10^3$. Further, we present ones that are representative of our data, have the correct (expected) curvature, and minimize the error functions well.

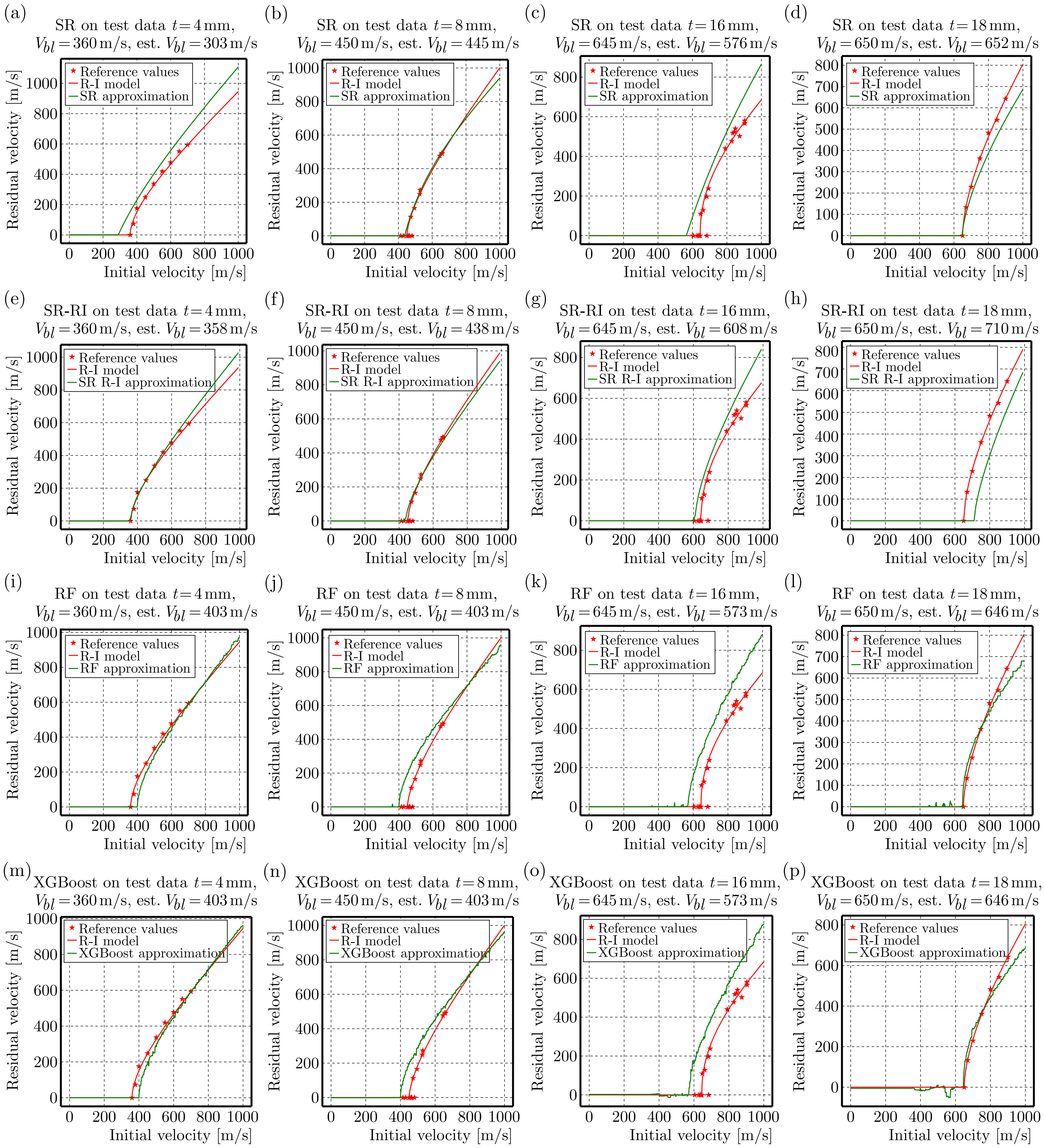

Fig. 3. Approximation of BLCs of all four ML methods trained on all but one thickness from our dataset that predict the shape BLC for the thickness that was not present in the dataset: (a)–(d) example results for SR; (e)–(h) for SR R-I; (i)–(l) for RF regressor, and (m)–(p) for XGBoost regressor. Red lines indicate the reference R-I model curve fitted to data marked as red stars, and green lines are the ML model approximation.

The equation approximated with SR for unknown $t = 8$ mm with RMSE = 17.674 on validation dataset for S355 steel valid in range $t \in [4, 18]$ mm is

$$h_{\mathrm{SR}}(v_i,t) = \left(\left(106.931^{\frac{215.235}{v_i}} - 1.566\right)\cdot\left(5.784^{(\log_{10}(t))^2}\right)\cdot(-12.323)\right) + v_i, \qquad t>0,\ v_i\neq 0, \tag{3.7}$$

$$\widehat{v_r}(v_i,t)_{\mathrm{SR}} = \begin{cases} h_{\mathrm{SR}}(v_i,t) & \text{if} \quad h_{\mathrm{SR}}(v_i,t)\geq 0,\\ 0 & \text{else.}\end{cases} \tag{3.8}$$

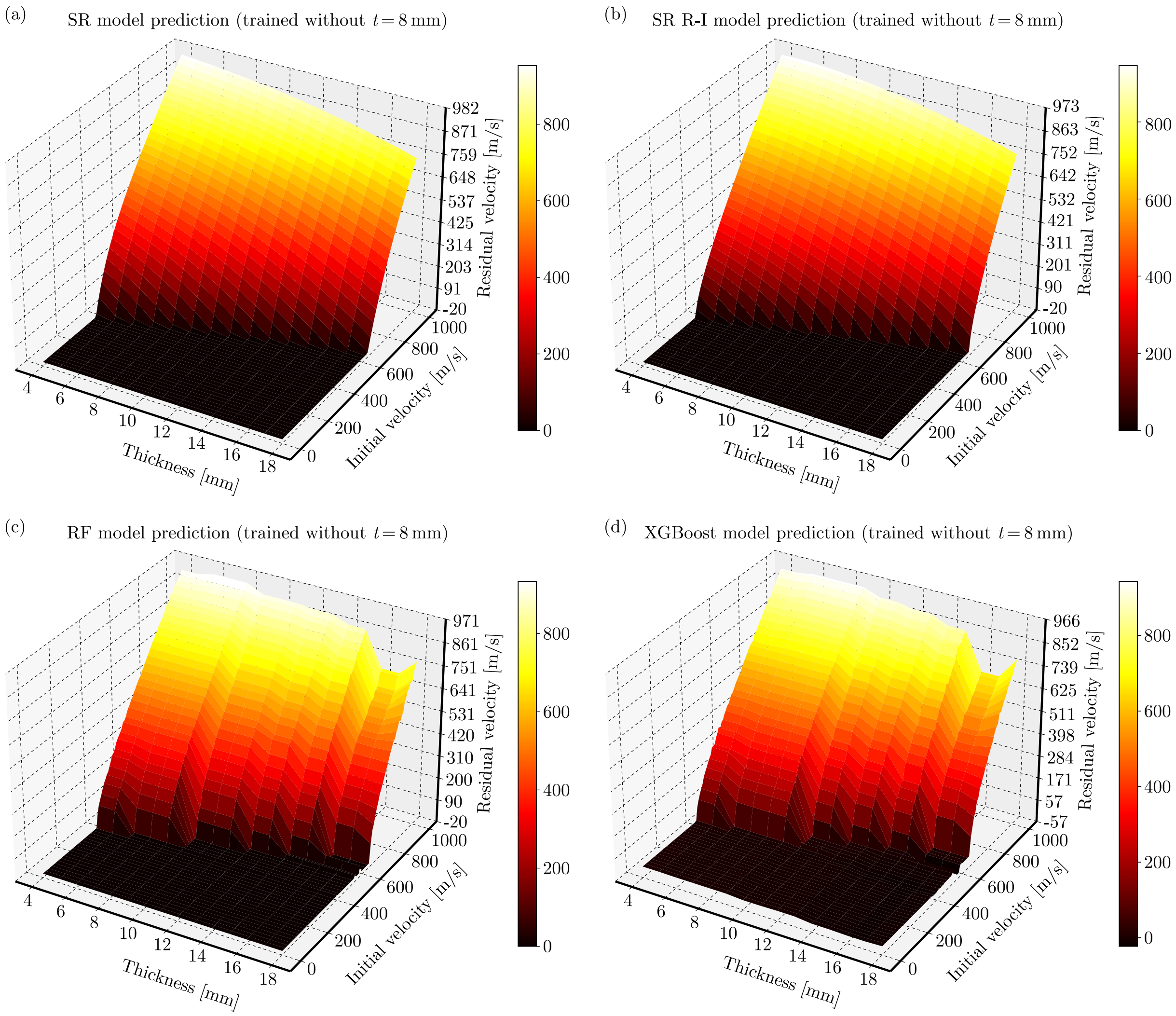

Fig. 4. Visualisations of $\widehat{v_r}(v_i, t)$ from Eq. (2.2) in the form of the surface plot: (a) is surface obtained with Eq. (3.8), (b) with Eq. (3.10), (c) with a RF regressor, (d) with an XGBoost regressor.

Note that this is a raw, not a physically meaningful, decomposition from SR.

In order to estimate BLV for a given t, one can use a heuristic that takes into consideration local monotonicity of $\widehat{v_r}$, a positive value of the first derivative, and a certain threshold (see (Hachaj & Frąś, 2026) for more details). The same heuristic was used for RF and XGBoost.

The equation approximated with SR R-I for unknown $t = 8$ mm with RMSE $= 26.153$ on the validation dataset for the steel S355 valid in the range $t \in [4, 18]$ mm is

$$\begin{cases} a(t) = t^{0.08}, \quad t \geq 0, \\ p(t) = 1.534, \\ v_{bl}(t) = (t + 12.697) \cdot 21.175, \end{cases} \tag{3.9}$$

and after applying Eq. (3.9) to Eq. (2.2) becomes:

$$\widehat{v_r}(v_i, t)_{\text{SR R-I}} = \begin{cases} t^{0.08} \cdot \left(v_i^{1.534} - ((t + 12.697) \cdot 21.175)^{1.534}\right)^{\frac{1}{1.534}} & \text{if} \quad v_i^{1.534} \geq ((t + 12.697) \cdot 21.175)^{1.534}, \\ 0 & \text{else.} \end{cases} \tag{3.10}$$

In order to estimate BLV for a given t one can directly use $v_{b\ell}(t)$ from Eq. (3.9). Note that the SR-derived function represents a smooth approximation (regularization effect) rather than a direct physical law. The primary objective is the accurate reconstruction of BLC/BLV rather than preserving parameter-level physical interpretation. Also, fixing $p(t)$ to a constant 1.534 removes a degree of freedom that the data clearly support. This might surely cause a loss of fit in the SR R-I compared to the situation in which p is allowed to depend on t.

4. Discussion

Based on the results presented in Table 2 and Table 3 and plots in Fig. 3, it may be observed that all evaluated ML methods generated the expected shapes of BLC. Those curves have relatively low error on experimental and numerical simulation data in leave-one-out cross-validation. It should be noted that in each case, validation data consist only of thicknesses that were not used in the training. Hence, a low error value indicates a strong generalization capability of the ML algorithms. We observe that SR algorithms (SR and SR R-I) perform very similarly, and decision tree-based algorithms (RF and XGBoost) also yield nearly identical errors. The lowest value of RMSE (51.656 $\pm$38.218) in the curve approximation task was achieved by SR, in the case of MAE (46.248 $\pm$44.058) by SR R-I, and in the case of R^2 by SR (0.908 $\pm$0.116). However, as shown in Table 4 and Table 5, the Wilcoxon test indicates that the difference between SR and SR R-I is not statistically significant. The RF and XGBoost perform significantly worse than SR, and there is no significant difference between the two decision tree-based methods. A similar conclusion can be drawn from evaluating how well models approximate BLV. Again, the SR R-I algorithm yielded the lowest error values: the MRE was 0.028 $\pm$0.029 (only 3 % $\pm$2 % of the reference values compared to other methods), RMSE was 25.678, MAE was 20.375, and R^2 was 0.934. However, according to Table 6 and Table 7, there are no significant statistical differences in RE and AE between SR methods, and they are statistically better than RF and XGBoost. Since our statistical tests approximate their resolution limit, their statistical power is modest, and the SR vs SR R-I comparison may be underpowered rather than truly null.

It should be noted that for the cases visualized in Fig. 3a and Fig. 3e, the SR approximation and SR R–I model seem to provide a nonphysical response, i.e., the residual velocity is higher than the initial velocity. This is evident at the ends of the interval under consideration, at the maximum value of the velocity v_i. This was likely because the model extrapolated the results to 4 mm. In contrast, the RF and XGBoost approaches exhibit nonphysical responses (lack of monotonicity), especially at the plateau near v_{bl}. This error stemmed from the nature of these models, which are aggregations of “weak” predictors.

The shapes of BLC generated by SR that are plotted in Fig. 3 indicate the monotonicity of the obtained solutions. In the case of RF and XGBoost, there are some fluctuations (characteristic steps in the plots) that are typical of decision tree-based algorithms. We can also observe those patterns in surface plots in Fig. 4. Equation (3.10) calculated by SR R-I is far more intuitive and easier to understand than Eqs. (3.7) and (3.8) done by SR. What is more, using Eq. (3.9), we can estimate BLV directly, which is not possible in other methods without the proposed heuristics. In summary, thanks to the SR R-I approach, we were able to compute analytical formulae for 2D BLCs over the range of material thickness for S355 Steel in ballistic events with 7.62 mm AP P80, which can be applied in engineering practice. When applying the Pareto front, the solution complexity is a trade-off for its accuracy. Often, a more complex solution containing more terms fits the dataset better than a simpler one. However, they might become less interpretable (see, for example, Eqs. (3.7) and (3.9)).

The application of a reliable, correctly fitted SR solution offers significant benefits over deep learning black-box models such as ANNs and larger language models (LLMs). The most important advantage is the full interpretability of the resulting solution, along with the ability to trace the process by which the result was obtained – something that is practically impossible in the case of deep learning. Furthermore, the resulting numerical function can be subjected to standard mathematical analysis to verify its consistency with physical assumptions, which is also practically impossible (or at least very difficult) for deep models with thousands or even millions of parameters. For this reason, interpretable knowledge distillation (Shmuel *et al.*, 2026) via SR ML is becoming an increasingly common practice in physical sciences (Varughese *et al.*, 2026).

There are several limitations of the proposed analytical solution. Equation (2.2) (and Eqs. (3.9) and (3.10)) takes into account the R-I model only through the term t, which corresponds to material thickness. Other parameters that might be interesting for this type of model include projectile type (the shape of the BLC curve also depends on the projectile's shape (Fonseca *et al.*, 2025)), target material properties, and the angle of impact. To include those parameters in the model, a series of experiments must be performed that covers all the variables. This is a necessary procedure for any ML-based model. We can anticipate that the modified, enhanced solution (Eq. (2.2)) that takes into account all those parameters should be in the form:

$$\begin{aligned}\widehat{v_r}(v_i,t,\alpha,\mathscr{P},\mathscr{M}) &= \mathscr{a}(t,\alpha,\mathscr{P},\mathscr{M})\cdot\left(v_i^{\mathscr{p}(t,\alpha,\mathscr{P},\mathscr{M})} - v_{\mathscr{b}\ell}(t,\alpha,\mathscr{P},\mathscr{M})^{\mathscr{p}(t,\alpha,\mathscr{P},\mathscr{M})}\right)^{\frac{1}{p(t,\alpha,\mathscr{P},\mathscr{M})}}, \\ v_i &\geq v_{\mathscr{b}\ell}(t,\alpha,\mathscr{P},\mathscr{M}),\end{aligned} \tag{4.1}$$

where α is an angle of impact (numerical value), $\mathscr{P}$, $\mathscr{M}$ are projectile and material properties (categorical values). It should be noted that the final solution will represent the $\mathscr{P}$, $\mathscr{M}$ as tabular-like categories rather than numerical values. We believe that the properties of materials and projectiles are too complex to be represented as single numerical values. Also, while applying the symbolic solution, it is not recommended to have more than four to five variables, because this is the border value above which the genetic algorithm can struggle to explore the search space effectively. With all these considerations taken into account, the model might become reliable for a wide range of materials and projectile types beyond S355 vs 7.62 mm $\times$ 51 mm AP P80 impacts at 0° NATO.

The main objective of this study was to investigate whether the R-I model can be generalized using SR methods. A particularly interesting research question is the minimum number of cross-sections required to obtain a stable (repeatable) solution with a given level of generalization and point-fit accuracy. In our case, we limited our tests to seven cross-sections in a leave-one-out evaluation, since conducting ballistic experiments is costly and simulating them using FEM requires significant computational resources over a relatively long period of time. To answer the question of how many cross-sections are necessary to estimate the function's variability, it depends on the form of the surface equation we expect. SR-based approximation differs fundamentally from, for example, polynomial interpolation, because in SR, we cannot state that to fit an n-th-degree polynomial, we need exactly $n+1$ points. Additionally, RL allows the use of various binary and unary operators, which can be treated as types of basis functions, significantly complicating the estimation of the required number of points. Based on our observations, seven curves appear to be sufficient to derive a model with satisfactory accuracy and low complexity for an approximately linear relationship. However, this number may prove insufficient for other materials or when additional parameters are included in the model (see Eq. (4.1)).

5. Conclusions

By applying SR, which embedded the R-I model within the PASR paradigm, we have obtained an intuitive and accurate solution which extends the original well-known equation. The SR R-I model performs with statistically proven effectiveness as SR and outperforms state-of-the-art RF and XGBoost approaches in both overall BLC fits and in predicting BLVs for unknown thicknesses. The obtained results confirmed the findings of our previous study (Hachaj & Frąś, 2026) that the application of stochastic physics-based oversampling enables us to generate a dataset large enough to train the repressor, providing sufficient points in a very narrow region near the BLV, which is critical for precise ML fit and prognostic ability of limit velocity values for unknown thicknesses. The proposed SR R–I model provides accurate interpolation within the training thickness range, with graceful degradation near boundary conditions. The results indicate that it is possible to use SR in selected terminal ballistic problems involving 355 steel targets penetrated by 7.62 mm AP P80, and to obtain explainable, interpretable solutions. The results may prove significant from scientific, cognitive, and practical engineering perspectives.

The SR R-I methodology we presented in this research is not limited to this specific material only, but can also be applied to other ballistic targets, and it is possible to find more general analytical formulae for many materials by applying parametric expressions to constraints. The other very promising research goal is to combine SR with LLMs. The initial research demonstrates that LLM integration consistently improves the reconstruction of physical dynamics from data, enhancing the robustness of SR models to noise and complexity (Fras & Pawlowski, 2026; Shen *et al.*, 2024; Taskin *et al.*, 2026). There are already publications on predicting the depth of the resulting crater following an impact. Rietkerk *et al.* (2023) and Ryan *et al.* (2024) modelled the impact of a long rod projectile at a given initial velocity into a semi-infinite target block using various ML approaches like XGBoost, ANN, support vector regression (SVR), Gaussian process regression, and physics-informed ML. As this represents a different experimental setup from that considered in the present study, we did not investigate it. Nevertheless, we consider it an interesting direction for future research.

References

1. Abid, K.A., Syed, S.A., & Khan, M. (2026). Interpretable machine learning models for predicting penetration depth in ultra-high-performance concrete under ballistic impact. *Structural Concrete*. https://doi.org/10.1002/suco.70462

2. Anderson Jr., C.E., & Bodner, S.R. (1988). Ballistic impact: The status of analytical and numerical modeling. *International Journal of Impact Engineering*, *7*(1), 9–35. https://doi.org/10.1016/0734-743X(88)90010-3

3. Cranmer, M. (2023). Interpretable machine learning for science with PySR and symbolic regression.jl. *arXiv*. https://doi.org/10.48550/arXiv.2305.01582

4. Deng, Y., Lv, Y., Yang, X., Du, C., & Huang, X. (2025). Determination of residual velocity model of finite thickness material based on Artificial Neural Network. *Thin-Walled Structures*, *216*(Part B), Article 113685. https://doi.org/10.1016/j.tws.2025.113685

5. Dwivedi, R., Dave, D., Naik, H., Singhal, S., Omer, R., Patel, P., Qian, B., Wen, Z., Shah, T., Morgan, G., & Ranjan, R. (2023). Explainable AI (XAI): Core ideas, techniques, and solutions. *ACM Computing Surveys*, *55*(9), Article 194. https://doi.org/10.1145/3561048

6. El Hasadi, Y.M.F., & Elghannay, H.A. (2026). A physics aware symbolic regression formula for the wall effects on a sphere moving inside a cylindrical tube. *International Journal of Multiphase Flow*, *198*, Article 105640. https://doi.org/10.1016/j.ijmultiphaseflow.2026.105640

7. European Committee for Standardization. (2019). *Hot rolled products of structural steels – Technical delivery conditions for non-alloy structural steels* (EN 10025-2:2019).

8. Fonseca, L.C., Peixoto, F.C., & Nichele, J. (2025). *Yaw-induced transitions in ballistic limit and fracture mechanisms in steel plate perforation* (version 1). Research Square. https://doi.org/10.21203/rs.3.rs-7767315/v1

9. Fras, T., & Pawlowski, P. (2026). On the applicability of generative artificial intelligence in modelling the dynamic behaviour of materials–potentials and pitfalls. *Journal of Dynamic Behavior of Materials*. https://doi.org/10.1007/s40870-025-00506-5

10. Frąś, T., Nowak, Z., Perzyna, P., & Pęcherski, R.B. (2011). Identification of the model describing viscoplastic behaviour of high strength metals. *Inverse Problems in Science and Engineering*, *19*(1), 17–30. https://doi.org/10.1080/17415977.2010.531474

11. Hachaj, T., & Frąś, T. (2026). Approximation of two-dimensional ballistic limit curves in the range of material thickness with stochastic physical-based oversampling. *Bulletin of the Polish Academy of Sciences Technical Sciences*, *74*(3), Article e158297. https://doi.org/10.24425/bpasts.2026.158297

12. Hachaj, T., & Piekarczyk, M. (2025). On explainability of reinforcement learning-based machine learning agents trained with proximal policy optimization that utilizes visual sensor data. *Applied Sciences*, *15*(2), Article 538. https://doi.org/10.3390/app15020538

13. Husain, A., Danish, M., Khan, S.H., & Mourad, A.-H.I. (2024). Predicting projectile residual velocities using an advanced artificial neural network model. *Heliyon*, *10*(11), Article e32149. https://doi.org/10.1016/j.heliyon.2024.e32149

14. Karl, J., Kirsch, F., Faderl, N., Perko, L., & Fras, T. (2020). Optimizing viscoelastic properties of rubber compounds for ballistic applications. *Applied Sciences*, *10*(21), Article 7840. https://doi.org/10.3390/app10217840

15. Karniadakis, G.E., Kevrekidis, I.G., Lu, L., Perdikaris, P., Wang, S., & Yang, L. (2021). Physics-informed machine learning. *Nature Reviews Physics*, *3*(6), 422–440. https://doi.org/10.1038/s42254-021- 00314-5

16. Lasdon, L.S., Fox, R.L., & Ratner, M.W. (1974). Nonlinear optimization using the generalized reduced gradient method. *R.A.I.R.O. Recherche opérationnelle*, *8*(V3), 73–103. https://doi.org/10.1051/ro/197408V300731

17. Levadnyi, I., Liu, F., & Gu, Y. (2024). Ballistic performance of TPU/steel configurations against spherical projectiles. *AIP Advances*, *14*(11), Article 115321. https://doi.org/10.1063/5.0239540

18. Li, W., Bian, Z., Chen, T., Mao, C., & Zhang, C. (2026). Reverse prediction of impact parameters for 3D woven fabrics subjected to ballistic impact using deep learning methods. *Mechanics of Advanced Materials and Structures*, *33*(1), Article 2569075. https://doi.org/10.1080/15376494.2025.2569075

19. Recht, R.F., & Ipson, T.W. (1963). Ballistic perforation dynamics. *Journal of Applied Mechanics*, *30*(3), 384–390. https://doi.org/10.1115/1.3636566

20. Rietkerk, R., Heine, A., & Riedel, W. (2023). Physics-informed machine learning model for prediction of long-rod penetration depth in a semi-infinite target. *International Journal of Impact Engineering*, *173*, Article 104465. https://doi.org/10.1016/j.ijimpeng.2022.104465

21. Rosenberg, Z., & Dekel, E. (2012). *Terminal ballistics*. Springer. https://doi.org/10.1007/978-3-642-25305-8

22. Ryan, S., Sushma, N.M., Kumar AV, A., Berk, J., Hashem, T., Rana, S., & Venkatesh, S. (2024). Machine learning for predicting the outcome of terminal ballistics events. *Defence Technology*, *31*, 14–26. https://doi.org/10.1016/j.dt.2023.07.010

23. Saifoori, S., Hosseinhashemi, S., Alasossi, M., Schilde, C., Nezamabadi, S., & Ghadiri, M. (2025). AI-assisted prediction of particle impact deformation simulated by material point method. *Powder Technology*, *459*, Article 121018. https://doi.org/10.1016/j.powtec.2025.121018

24. Shen, J., Tenenholtz, N., Hall, J.B., Alvarez-Melis, D., & Fusi, N. (2024). Tag-LLM: Repurposing general-purpose LLMs for specialized domains. *Proceedings of the 41st International Conference on Machine Learning*, *235*, 44759–44773.

25. Shmuel, A., Koren, N., Glickman, O., & Lazebnik, T. (2026). Interpretable knowledge distillation via symbolic regression for feedforward neural networks. *Neural Computing and Applications*, *38*(7), Article 243. https://doi.org/10.1007/s00521-026-12067-2

26. Taskin, B., Xie, W., & Lazebnik, T. (2026). Knowledge integration for physics-informed symbolic regression using pre-trained large language models. *Scientific Reports*, *16*, Article 1614. https://doi.org/10.1038/s41598-026-35327-6

27. Varughese, B., Loeffler, T.D., Banik, S., Koneru, A., Manna, S., Balasubramanian, K., Batra, R., Cherukara, M.J., Yildiz, O., Peterka, T., Sumpter, B.G., & Sankaranarayanan, S.K.R.S. (2026). Physically interpretable interatomic potentials via symbolic regression and reinforcement learning. *npj Computational Materials*, *12*, Article 84. https://doi.org/10.1038/s41524-025-01952-4

28. Wei, Q., Chen, J., Liu, Y., & Zhang, H. (2024). Numerical analysis of ballistic performance in hybrid structures of triaxial and plain fabrics. *Journal of Materials Science*, *59*(45), 21069–21086. https://doi.org/10.1007/s10853-024-10445-6

29. Zhang, L., Zhang, Z., Zhang, Y., Chen, L., Li, S., Zhu, L., Ye, Y., Chen, R., & Bai, S. (2026). Machine learning driven impact fracture understanding and end-to-end design of energetic multi-principal-element alloys. *Defence Technology*, *59*, 217–230. https://doi.org/10.1016/j.dt.2025.11.026

30. Zou, D., Thoti, D., & Bao, Z. (2025). Study on the application of discrepancy-guided symbolic regression algorithm in analyzing the impact resistance of UHP-SFRC target against high velocity projectile impact. *International Journal of Impact Engineering*, *201*, Article 105276. https://doi.org/10.1016/j.ijimpeng.2025.105276

Manuscript received March 26, 2026; accepted for publication July 4, 2026; published online August 17, 2026.